

Decreased monsoon precipitation in the Northern Hemisphere due to anthropogenic aerosols

Article

Supplemental Material

Polson, D., Bollasina, M., Hegerl, G. C. and Wilcox, L. J.
ORCID: <https://orcid.org/0000-0001-5691-1493> (2014)
Decreased monsoon precipitation in the Northern Hemisphere
due to anthropogenic aerosols. *Geophysical Research Letters*,
41 (16). pp. 6023-6029. ISSN 1944-8007 doi:
<https://doi.org/10.1002/2014GL060811> Available at
<https://centaur.reading.ac.uk/37376/>

It is advisable to refer to the publisher's version if you intend to cite from the work. See [Guidance on citing](#).

Published version at: <http://onlinelibrary.wiley.com/doi/10.1002/2014GL060811/abstract>

To link to this article DOI: <http://dx.doi.org/10.1002/2014GL060811>

Publisher: American Geophysical Union

All outputs in CentAUR are protected by Intellectual Property Rights law, including copyright law. Copyright and IPR is retained by the creators or other copyright holders. Terms and conditions for use of this material are defined in the [End User Agreement](#).

www.reading.ac.uk/centaur

CentAUR

Central Archive at the University of Reading

Reading's research outputs online

1 **Auxiliary material for:**
2 **Decreased monsoon precipitation in the**
3 **Northern Hemisphere due to anthropogenic aerosols**

4
5 **Geophysical Research Letters**

6
7 *D. Polson, M. Bollasina, G. C. Hegerl and L. J. Wilcox*
8

9 *a. 2-signal detection and attribution results*

10 Figure S1 shows the results of a 2-signal detection and attribution analysis for combi-
11 nations of anthropogenic aerosol and natural forcings (AA&NAT) and greenhouse gas and
12 natural forcing (GHG&NAT) as described in the main the paper.

13 *b. Spatial precipitation patterns in NHSM region*

14 Figure S2 shows spatial linear trend patterns for MJJAS precipitation for observations
15 (GPCC) and the multi-model mean for each individual forcing. The spatial pattern of ALL
16 and ANT are more consistent with the AA than the GHG multi-model mean. GHG multi-
17 model mean shows increasing precipitation over most of the NHSM region, while the AA
18 multi-model means shows mostly drying trends. The observed trends show an increase in
19 precipitation over the whole period over South America and parts of Asia, while the ALL
20 multi-model mean shows a decrease in precipitation in these regions. Conversely, in parts of
21 Africa, the ALL multi-model mean has increasing precipitation while the observations show
22 an overall decrease, though the models do not tend to show much consistency in the sign of
23 the trends (less than 2/3 of simulations have trends of the same sign). However the timeseries
24 for the observed mean precipitation in the NHSM region (Figs S3-S6) show that precipitation

25 decreases from 1951, reaches a minimum in the mid-1980s and then begins to recover, with
26 the observed recovery greater in Asia than Africa, a behaviour not well captured by a linear
27 trend. While ALL seems to capture the general decrease in precipitation from the 1950s to
28 1980s, during the 1990s, it tends to underestimate the recovery over Asia and overestimate
29 the recovery over Africa.

30 The role of the indirect aerosol effect is investigated by plotting the multi-model mean
31 trends and timeseries for the ALL forced models that included both the indirect and direct
32 effects and the models that include the direct effect only (Figs. S2 and S3). The mean
33 precipitation change for the whole region is largely the same for both ensembles. However
34 the spatial trend patterns show interesting differences, particularly over Asia. The models
35 that include the indirect effect tend to simulate drier conditions over India and central China
36 than the models that include the direct effect only. These results suggest that the relative
37 influence of the indirect and direct effects on precipitation in the models varies between
38 regions.

39 The spatial trend patterns are also plotted for 1951-1985 and 1985-2005 (Figure S7 and
40 S8). The spatial trend pattern for 1951-1985 is similar for the ALL forced multi-model
41 mean and observations, with both showing largely decreasing precipitation from the 1950s
42 to mid-1980s. The ANT and AA multi-model means also show a similar pattern, suggesting
43 that aerosols are at least in part responsible for this decrease. However the increase in
44 precipitation in Africa from 1985-2005 is overestimated by the ALL forced multi-model,
45 while the pattern of increasing precipitation over East Asia and decreasing precipitation
46 over India is not reproduced by the ALL forced multi-model mean, though the AA forced
47 multi-model mean does give a similar pattern. There is, however, little consistency between
48 ALL forced simulations on the sign of the trends from 1985-2005.

49 To highlight the variability between simulated trends from 1951-2005, we calculate an
50 error score, Sk , for each individual model simulation compared to observations using

$$Sk = rmse + N_{err} \quad (1)$$

51 where *rmse* is root mean square error of simulated trends with respect to the observations
52 and N_{err} is the number of grid boxes where the sign of the trend disagrees with observations.
53 Both *rmse* and N_{err} are calculated as a fraction of the mean of values for all simulations.
54 Figures S9 and S10 show the 1951-2005 trends for the 6 simulations with the most and least
55 agreement with the observations. Note this is not an assessment of model performance, rather
56 the aim is to demonstrate the variability of the trend patterns between simulations, hence
57 we use individual model simulations, not model ensembles. No single simulation perfectly
58 reproduces the observed trends in all regions (shown in Figure S2), however the observed
59 increase/decrease in precipitation in each region is simulated by more than one of the 'best'
60 simulations. The 'worst' simulations all fail to fully reproduce the decrease in precipitation
61 over Africa, but do tend to capture the drying trends over east Asia. The multi-model mean
62 trends for an ensemble of ALL forced models that uses only one simulation per modelling
63 group (as opposed to all simulations available used in the main results), shows that the trend
64 patterns do not appear to be biased to any one model or modelling centre (not shown).

65 *c. Sensitivity of detection and attribution results*

66 The inconsistency in the observed and model spatial trend patterns over the period 1951-
67 2005 does not seem to affect the detection and attribution results for the mean temporal
68 signal for the whole region. This may be due to a coincidental cancellation of the positive
69 and negative changes in different regions. However, it is more likely that while the models
70 capture most of the temporal variation over this period, the recent increase in precipitation
71 over many regions is not captured correctly by the models. This may be because the observed
72 changes are simply due to internal climate variability, because the forcings in the models
73 are not consistent with reality, because of uncertainty in the observations or a combination

74 of these factors. To check the sensitivity of the results to the exclusion of different regions,
75 the analysis was also repeated excluding first South America (supplementary Figure S11(a)),
76 then Africa (supplementary Figure S11(b)) and finally Asia (supplementary Figure S11(c)).
77 In each case the results are broadly similar to those for the whole region. The analysis
78 was also repeated to verify whether the results were sensitive to the inclusion of the mid-
79 latitude NHSM region. The 3-signal analysis shows similar detection of AA forcing when
80 the mid-latitudes NHSM regions are included (Figure S11(d)).

81 The detection and attribution analysis was also repeated using the same model ensemble
82 for each pair of forcings in the 2-signal analysis (Figs. S12(a)-(d)) and for the GHG, NAT
83 and AA forcing in the 3-signal analysis (Figure S12(e)). The detection results for different
84 forcings are identical to the results using all available models and are therefore not sensitive
85 to the model ensemble (see *Zhang et al. (2007)*).

86 **Linearity of the individual forcings**

87 In the above the analysis, we assumed that the combined influence of all external forcings
88 can be well approximated by a linear combination of individual forcings, and that by adding
89 the contribution of GHG, AA and NAT, we can reproduce the changes in precipitation from
90 the ALL forced simulations (i.e. ignoring the influence of other forcings such as land use
91 change). To check if this is a reasonable assumption we compare the ALL multi-model mean
92 to the sum of GHG, NAT and AA multi-model means (Figure S13(a)), using the method de-
93 scribed in Schurer et al. (*Schurer et al. 2014*). Subtracting the sum of GHG+NAT+AA from
94 ALL, gives the residual shown in Figure S13(b). If the forcings add linearly, then the residual
95 and the internal variability should be consistent. The internal variability is calculated from
96 the samples of noise derived from the ALL forcing ensemble as described in the methods
97 section. The standard deviation is calculated for each member of the noise ensemble and
98 as model simulations have different internal variability, we use the mean standard deviation

99 for the whole ensemble to check the consistency of the residual with internal variability. If
100 the residual is within 2 standard deviations of the internal variability, then we can say that
101 the assumption of linearity has not been disproven. The results show that the assumption
102 of linearity has not been violated.

103 *d. Observational versus model variability*

104 To check that the variability in the models is consistent with the observed variability,
105 the variance for MMJAS precipitation was calculated for South America, Africa and Asia,
106 for each observational dataset and every simulation in the ALL ensemble. Figure S14 shows
107 the range of the ratio of the variance between the observational datasets and each individual
108 model simulation. The results for both the unsmoothed and 9-year smoothed precipitation,
109 show that the models tend to underestimate the variance in the observations, though in
110 most cases a variance ratio of 1 is within the 90% confidence interval. Only for Africa, for
111 the 9-year smoothed data, does the 90% confidence interval exceed 1. However doubling the
112 model variance, as done when calculating the noise samples for the detection and attribution
113 analysis, gives a variance ratio of 1 within the 90% confidence interval. Note that the
114 detection and attribution results remain valid if the African monsoon region is excluded
115 (Figure S11).

116

117 REFERENCES

118 Schurer, A. P., S. F. B. Tett, and G. C. Hegerl (2014), Small influence of solar variability on
119 climate over the past millennium, *Nature Geosci*, 7, 104–108.

- 120 Taylor, K. E., R. J. Stouffer, and G. A. Meehl (2011), An Overview of CMIP5 and the
121 Experiment Design, *Bull. Amer. Meteor. Soc.*, *93*, 485–498.
- 122 Zhang, X., et al. (2007), Detection of human influence on twentieth-century precipitation
123 trends, *Nature*, *448*(7152), 461–465.

124 List of Tables

125	1	List of models and numbers of simulations used in this analysis (<i>Taylor et al.</i>	
126		2011).	8

TABLE 1. List of models and numbers of simulations used in this analysis (*Taylor et al.* 2011).

<i>InstituteID</i>	<i>ModelName</i>	<i>ALL</i>	<i>ANT</i>	<i>GHG</i>	<i>AA</i>	<i>NAT</i>	<i>IND + DIR</i>	<i>DIR</i>
BCC	BCC-CSM1.1	4				1		4
CCCMA	CanESM2	5		5	4	5	5	
CMCC	CMCC-CESM	1					1	
CMCC	CMCC-CMS	1					1	
CMCC	CMCC-CM	1					1	
CNRM-CERFACS	CNRM-CM5	5		5		5	5	
EC-EARTH	EC-EARTH	4						
FIO	FIO-ESM	1						
NASA GISS	GISS-E2-H	5	4	5	1	5	5	
NASA GISS	GISS-E2-H-CC	1					1	
NASA GISS	GISS-E2-R	5	2	5	1	5	5	
MOHC	HadGEM2-ES	4		4		4	4	
MOHC	HadGEM2-CC	1					1	
MOHC	HadCM3	5					5	
INM	INM-CM4	2						
IPSL	IPSL-CM5A-LR	4	3	5		1	4	
IPSL	IPSL-CM5A-MR	1		3		3	1	
NCC	NorESM1-M	3		1	1	1	3	
NCC	NorESM1-ME	1					1	
CSIRO-QCCCE	CSIRO-Mk3.6.0	5	5	5	5	5	5	
CSIRO-BOM	ACCESS1.0	1					1	
NOAA GFDL	GFDL-ESM2G	5						5
NOAA GFDL	GFDL-ESM2M	2	1			1		2
NOAA GFDL	GFDL-CM3	5	3	3	3	3	5	
MIROC	MIROC5	3					3	
MIROC	MIROC-ESM	3		1		1	3	
MIROC	MIROC-ESM-CHEM	1		1		1	1	
MPI-M	MPI-ESM-LR	3						3
MRI	MRI-CGCM3	5		1		1	5	
NCAR	CCSM4	5		3		3		5
NSF-DOE-NCAR	CESM1(BGC)	2						2
NSF-DOE-NCAR	CESM1(CAM5)	3					3	
NSF-DOE-NCAR	CESM1(CAM5.1,FV2)	4		2		2	4	
NSF-DOE-NCAR	CESM1(FASTCHEM)	3					3	
NSF-DOE-NCAR	CESM1(WACCM)	1						1

128 S1 Detection and attribution results for observed changes in Northern Hemi-
129 sphere Summer monsoon precipitation. (a), 2-signal regression for anthro-
130 pogenic aerosol (AA) and natural (NAT) forcing. (b), 2-signal regression for
131 greenhouse gas (GHG), and natural (NAT) forcing. Results are shown for
132 four observational datasets, CRU (CRU), Zhang (ZHA), VasClimO (VAS)
133 and GPCP (GPCP). Crosses show the best-guess scaling factor for the multi-
134 model mean, thick lines are the 90% confidence interval based on the raw
135 variance and thin lines are the 90% confidence intervals when model vari-
136 ance has been doubled. The residual consistency test is passed for all cases.
137 Stars (*) show where forcing is detected and two stars show where forcing is
138 detected but inconsistent with a scaling factor of 1. 14

139 S2 Observed and multi-model mean model MJJAS precipitation linear trends
140 (mm/month/year) for 1951-2005. Shown are for all external forcings (ALL),
141 observed (GPCP), all forced models that include both the indirect and direct
142 effects (ALL(indirect+direct)), all forced models that only include the direct
143 effect (ALL(direct)), greenhouse gas forcing (GHG), natural forcings (NAT),
144 anthropogenic forcings (ANT) and anthropogenic aerosol forcing (AA). Hatch-
145 ing shows where over 2/3 of individual simulations produce trends of the same
146 sign. Information on whether the indirect effect is included was not avail-
147 able for all models so the combined ensemble of ALL(indirect+direct) +
148 ALL(direct) is less than ALL, explaining any inconsistencies in the hatch-
149 ing. 15

- 150 S3 As Figure 1 but for ALL(indirect+direct) and ALL(direct) ensembles. Shown
151 are the timeseries for the GPCC observational dataset and the multi-model
152 mean for all external forcings (ALL), the all external forcing scaled by the
153 GPCC total least squares scaling factor (ALL scaled), the multi-model mean
154 all forced models that include the indirect and direct effects (ALL(indirect+direct))
155 and models that include the direct effect only (ALL(direct)). Orange shading
156 shows the 5%-95% range for the ALL ensemble. Models are masked to the
157 GPCC dataset. 16
- 158 S4 As Figure 1 for the South American NHSM region. Shown are for 4 ob-
159 servations datasets, CRU, Zhang, VasClimO and GPCC and multi-model
160 mean for all external forcings (ALL), greenhouse gas forcing (GHG), an-
161 thropogenic aerosol forcing (AA), natural forcing (NAT) and anthropogenic
162 forcings (ANT). Note multi-model means are plotted on a different scale to
163 observations. Orange shading shows the 5%-95% range for the ALL ensemble,
164 plotted on the same scale as observations. Models are masked to the GPCC
165 dataset. 17
- 166 S5 As Figure 1 for the African NHSM region. Shown are 4 observations datasets,
167 CRU, Zhang, VasClimO and GPCC and multi-model mean for all external
168 forcings (ALL), greenhouse gas only forcing (GHG), anthropogenic aerosol
169 only forcing (AA), natural only forcing (NAT) and anthropogenic forcings
170 (ANT). Note multi-model means are plotted on a different scale to observa-
171 tions. Orange shading shows the 5%-95% range for the ALL ensemble, plotted
172 on the same scale as observations. Models are masked to the GPCC dataset. 18

173 S6 As Figure 1 for the Asian NHSM region. Shown are 4 observations datasets,
174 CRU, Zhang, VasClimO and GPCC and multi-model mean for all external
175 forcings (ALL), greenhouse gas only forcing (GHG), anthropogenic aerosol
176 only forcing (AA), natural only forcing (NAT) and anthropogenic forcings
177 (ANT). Note multi-model means are plotted on a different scale to observa-
178 tions. Orange shading shows the 5%-95% range for the ALL ensemble, plotted
179 on the same scale as observations. Models are masked to the GPCC dataset. 19

180 S7 Figure S2 except precipitation linear trends (mm/day/year) are for 1951-1985. 20

181 S8 As Figure S2 except precipitation linear trends (mm/day/year) are for 1985-
182 2005. 21

183 S9 Linear trends for simulations that best agree with observations. ALL forced
184 simulation MJJAS precipitation linear trends (mm/day/year) for 1951-2005
185 for the 6 simulations that best agree with observations (lowest error score). 22

186 S10 Linear trends for simulations with least agreement with observations. ALL
187 forced simulation MJJAS precipitation linear trends (mm/day/year) for 1951-
188 2005 for 6 simulations with least agreement with observations (highest error
189 score). 23

190 S11 Detection and attribution results for observed changes in NHSM precipita-
191 tion testing for overweighting of individual regions. Shown are the 3-signal
192 analysis results for greenhouse gas (GHG), natural (NAT) and anthropogenic
193 aerosol (AA) forcing for the NHSM region (a)-(c), excluding South American,
194 African and Asian monsoon regions and (d), including the mid-latitude re-
195 gions. Results are shown for four observational datasets, CRU (CRU), Zhang
196 (ZHA), VasClimO (VAS) and GPCC (GPCC). Crosses show the best-guess
197 scaling factor for the multi-model mean, thick lines are the 90% confidence
198 interval based on the raw variance and thin lines are the 90% confidence in-
199 tervals when model variance has been doubled. The residual consistency test
200 is passed for all cases. Stars (*) show where forcing is detected and two stars
201 show where forcing is detected but inconsistent with a scaling factor of 1. 24

202 S12 Detection and attribution results for observed changes in NHSM precipitation
203 where the same models are used to produce the fingerprint for each combina-
204 tion of forcings. (a)-(d), 2-signal and (e), 3-signal detection and attribution
205 analysis. (a), anthropogenic (ANT) and natural (NAT) forcing, (b), anthro-
206 pogenic aerosol (AA) and natural (NAT) forcing, (c), anthropogenic aerosol
207 (AA) and greenhouse gas (GHG) forcing, (d), greenhouse gas (GHG) and
208 natural (NAT) forcing and (e), greenhouse gas (GHG), natural (NAT) and
209 anthropogenic aerosol (AA) forcing. Results are shown for four observational
210 datasets, CRU (CRU), Zhang (ZHA), VasClimO (VAS) and GPCC (GPCC).
211 Crosses show the best-guess scaling factor for the multi-model mean, thick
212 lines are the 90% confidence interval based on the raw variance and thin lines
213 are the 90% confidence intervals when model variance has been doubled. The
214 residual consistency test is passed for all cases. Stars (*) show where forcing
215 is detected and two stars show where forcing is detected but inconsistent with
216 a scaling factor of 1. 25

217 S13 Test of linearity assumption (a), The ALL multi-model mean and the sum
218 of GHG+NAT+AA multi-model means for the NHSM region. (b), Residual
219 (ALL multi-model mean minus the summed GHG+NAT+AA multi-model
220 means). Dashed lines show 2 standard deviations of the internal variability
221 from noise sample ensemble derived from the ALL forcing ensemble. 26

222 S14 Comparison of observed and modelled variance. Ratio of observed and ALL
223 forced model simulations mean MJJAS precipitation variance for each region,
224 SA is South America, AF is Africa and AS is Asia) and each observational
225 datasets (c is CRU, z is Zhang v is VasClimO and g is GPCC). (a) unsmoothed,
226 (b) 9-year running mean. The crosses show the median value and the bars
227 are the 90% confidence interval. Dashed lines shows ratio of 1 and dotted line
228 shows ratio of 2. 27

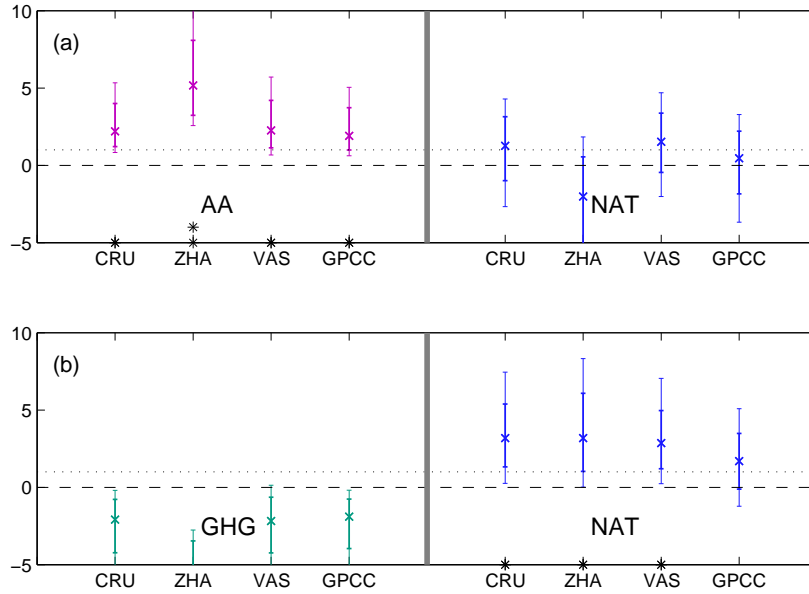


FIG. S1. Detection and attribution results for observed changes in Northern Hemisphere Summer monsoon precipitation. (a), 2-signal regression for anthropogenic aerosol (AA) and natural (NAT) forcing. (b), 2-signal regression for greenhouse gas (GHG), and natural (NAT) forcing. Results are shown for four observational datasets, CRU (CRU), Zhang (ZHA), VasClimO (VAS) and GPCC (GPCC). Crosses show the best-guess scaling factor for the multi-model mean, thick lines are the 90% confidence interval based on the raw variance and thin lines are the 90% confidence intervals when model variance has been doubled. The residual consistency test is passed for all cases. Stars (*) show where forcing is detected and two stars show where forcing is detected but inconsistent with a scaling factor of 1.

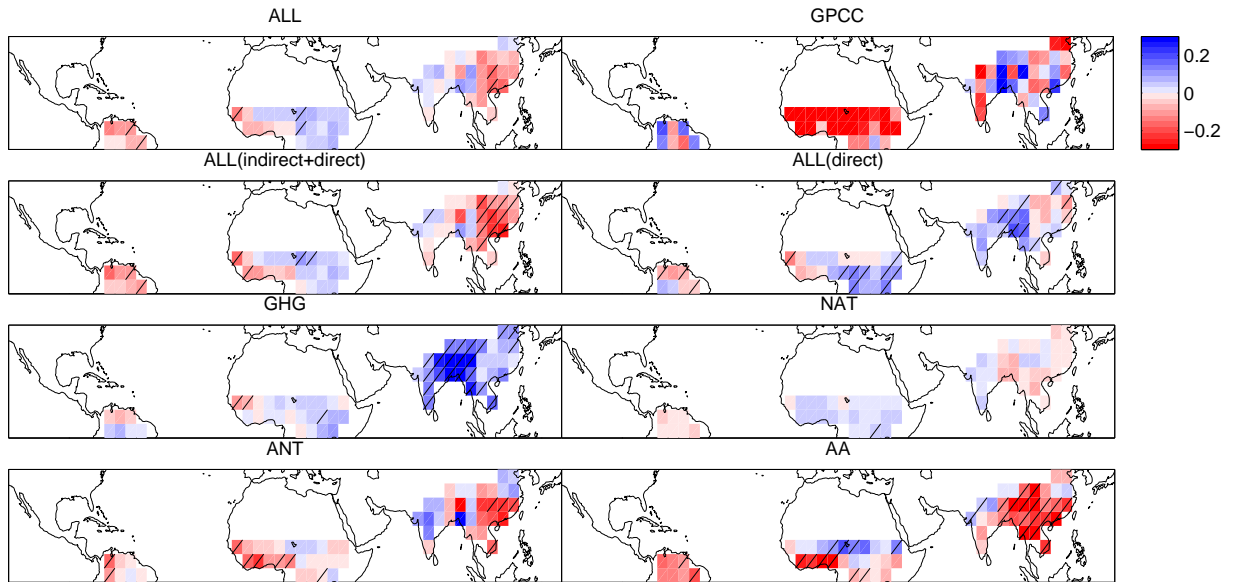


FIG. S2. Observed and multi-model mean model MJJAS precipitation linear trends (mm/month/year) for 1951-2005. Shown are for all external forcings (ALL), observed (GPCC), all forced models that include both the indirect and direct effects (ALL(indirect+direct)), all forced models that only include the direct effect (ALL(direct)), greenhouse gas forcing (GHG), natural forcings (NAT), anthropogenic forcings (ANT) and anthropogenic aerosol forcing (AA). Hatching shows where over 2/3 of individual simulations produce trends of the same sign. Information on whether the indirect effect is included was not available for all models so the combined ensemble of ALL(indirect+direct) + ALL(direct) is less than ALL, explaining any inconsistencies in the hatching.

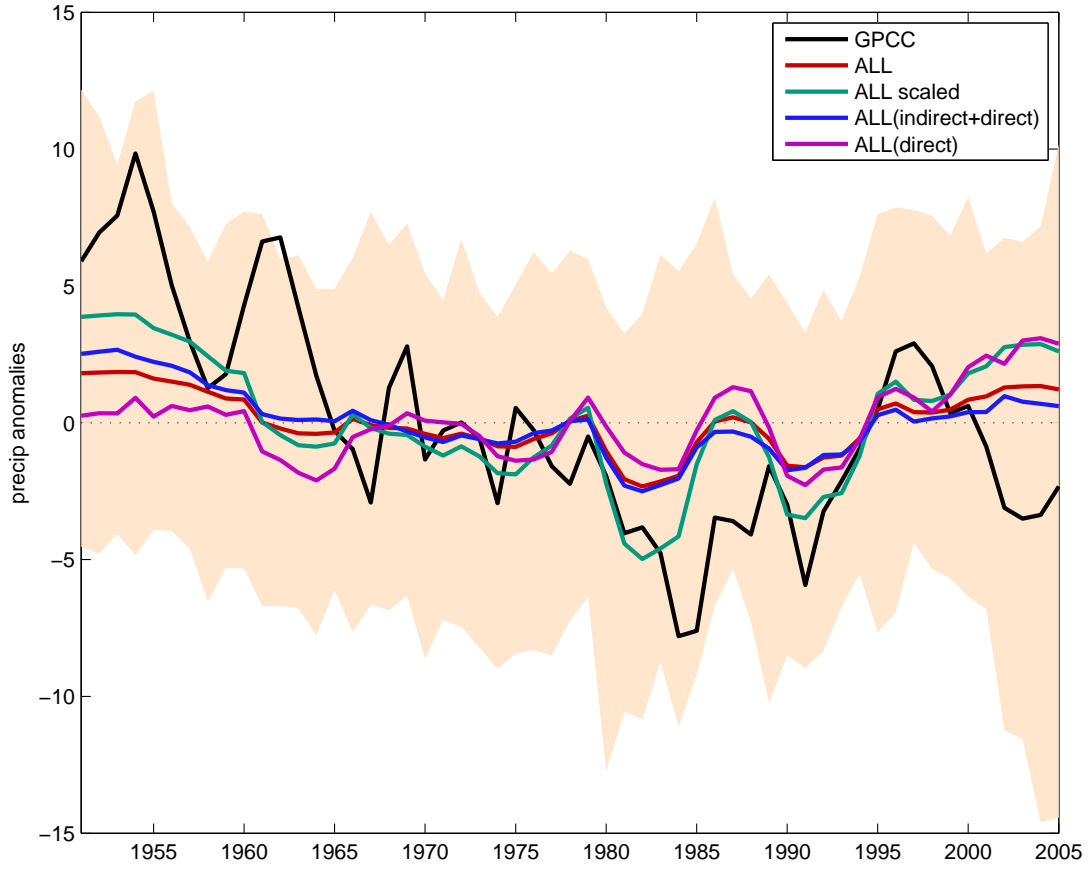


FIG. S3. As Figure 1 but for ALL(indirect+direct) and ALL(direct) ensembles. Shown are the timeseries for the GPCC observational dataset and the multi-model mean for all external forcings (ALL), the all external forcing scaled by the GPCC total least squares scaling factor (ALL scaled), the multi-model mean all forced models that include the indirect and direct effects (ALL(indirect+direct)) and models that include the direct effect only (ALL(direct)). Orange shading shows the 5%-95% range for the ALL ensemble. Models are masked to the GPCC dataset.

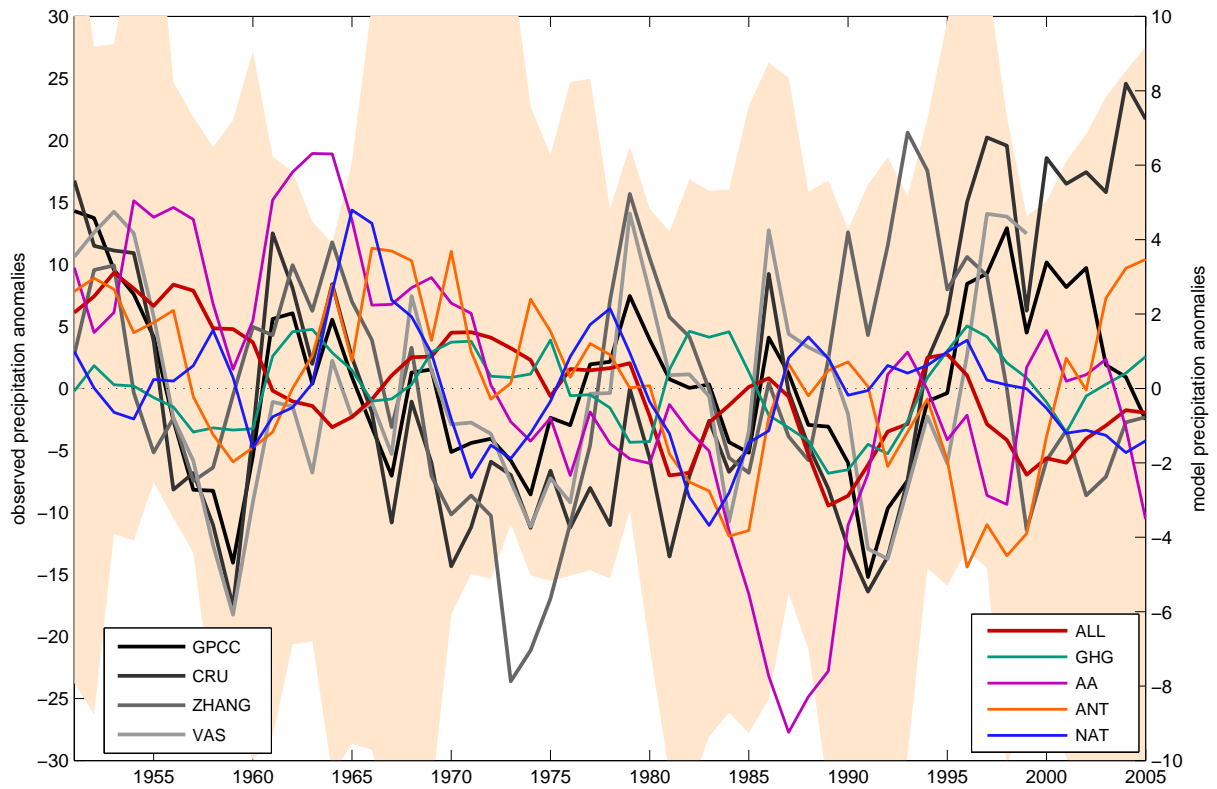


FIG. S4. As Figure 1 for the South American NHSM region. Shown are for 4 observations datasets, CRU, Zhang, VasClimO and GPCC and multi-model mean for all external forcings (ALL), greenhouse gas forcing (GHG), anthropogenic aerosol forcing (AA), natural forcing (NAT) and anthropogenic forcings (ANT). Note multi-model means are plotted on a different scale to observations. Orange shading shows the 5%-95% range for the ALL ensemble, plotted on the same scale as observations. Models are masked to the GPCC dataset.

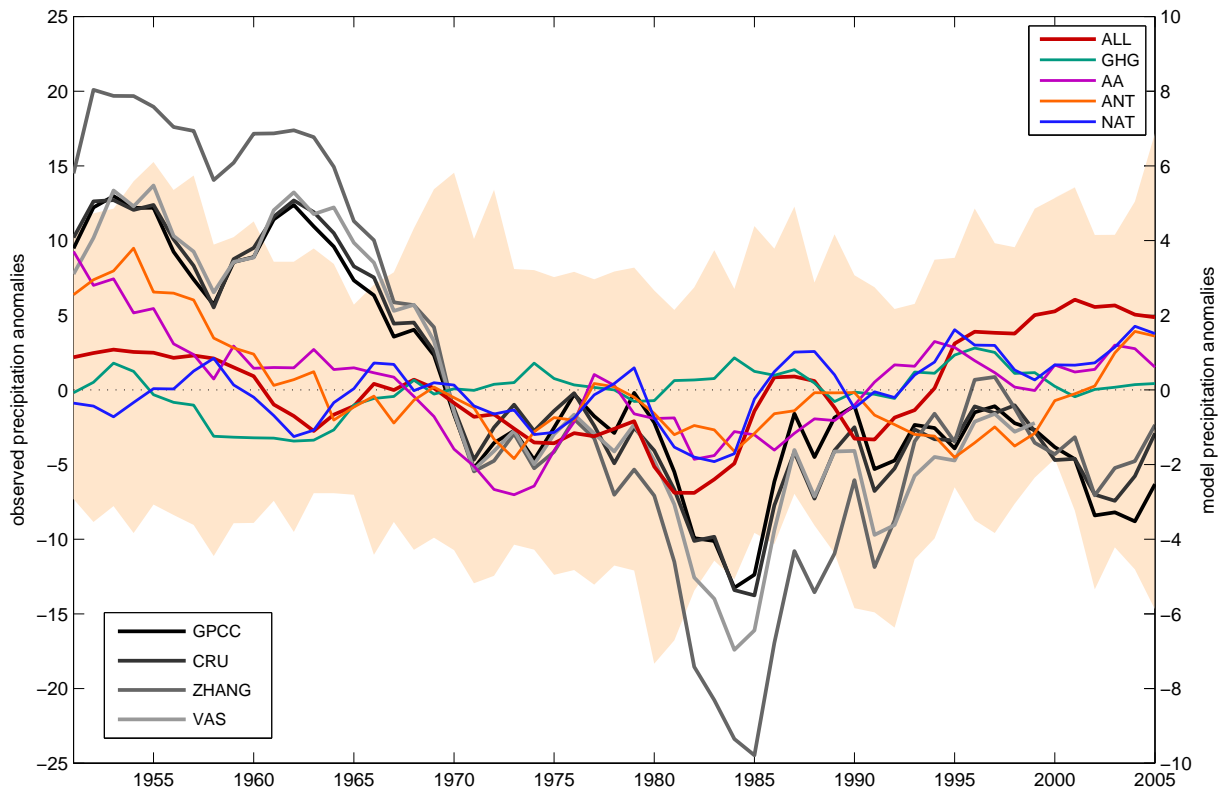


FIG. S5. As Figure 1 for the African NHSM region. Shown are 4 observations datasets, CRU, Zhang, VasClimO and GPCC and multi-model mean for all external forcings (ALL), greenhouse gas only forcing (GHG), anthropogenic aerosol only forcing (AA), natural only forcing (NAT) and anthropogenic forcings (ANT). Note multi-model means are plotted on a different scale to observations. Orange shading shows the 5%-95% range for the ALL ensemble, plotted on the same scale as observations. Models are masked to the GPCC dataset.

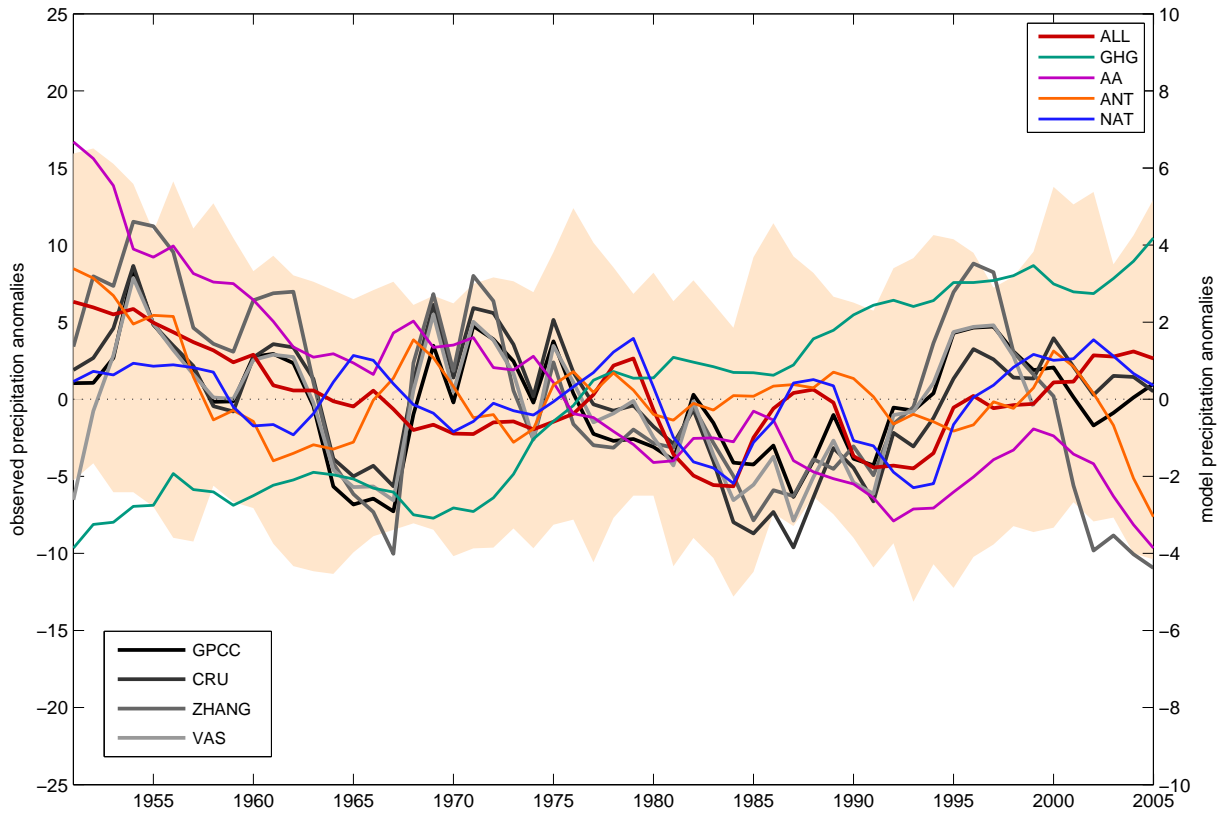


FIG. S6. As Figure 1 for the Asian NHSM region. Shown are 4 observations datasets, CRU, Zhang, VasClimO and GPCCC and multi-model mean for all external forcings (ALL), greenhouse gas only forcing (GHG), anthropogenic aerosol only forcing (AA), natural only forcing (NAT) and anthropogenic forcings (ANT). Note multi-model means are plotted on a different scale to observations. Orange shading shows the 5%-95% range for the ALL ensemble, plotted on the same scale as observations. Models are masked to the GPCCC dataset.

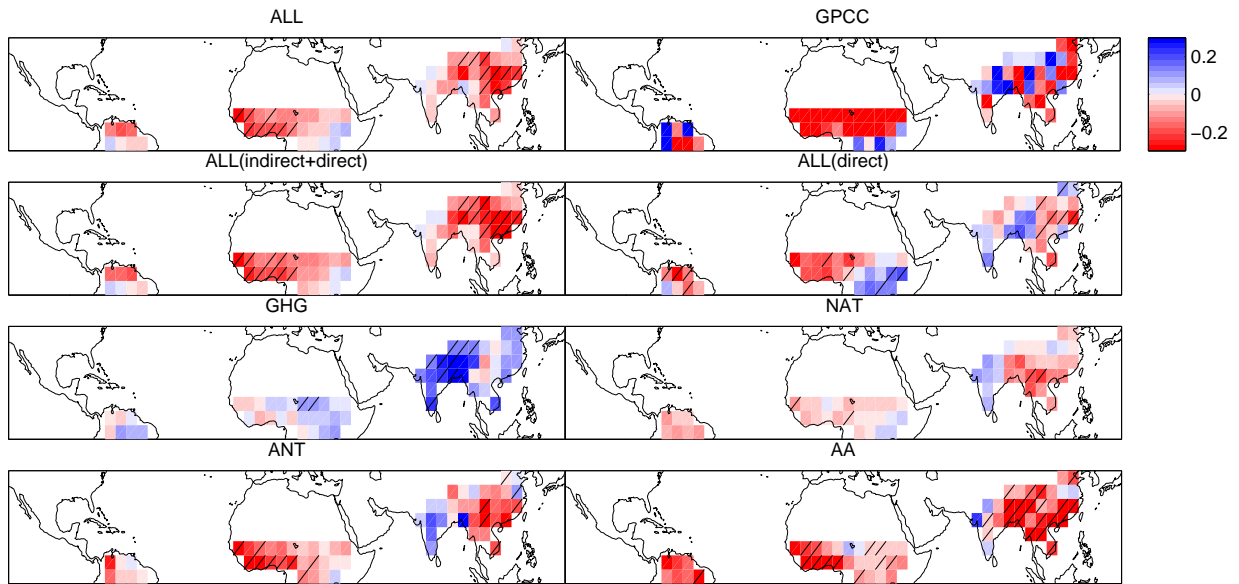


FIG. S7. Figure S2 except precipitation linear trends (mm/day/year) are for 1951-1985.

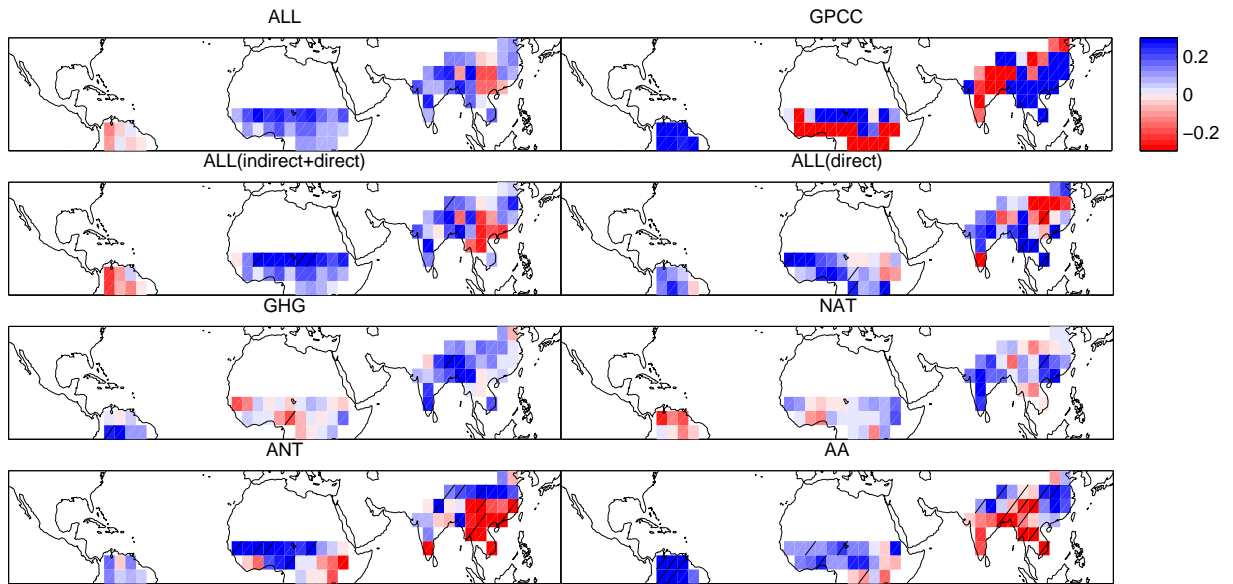


FIG. S8. As Figure S2 except precipitation linear trends (mm/day/year) are for 1985-2005.

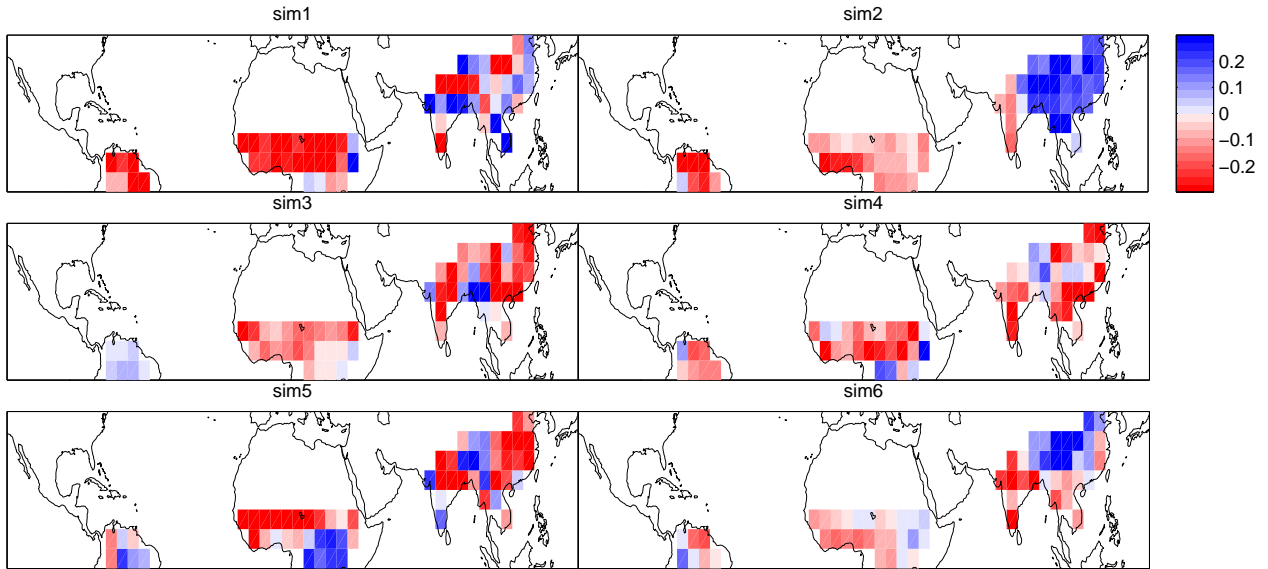


FIG. S9. Linear trends for simulations that best agree with observations. ALL forced simulation MJJAS precipitation linear trends (mm/day/year) for 1951-2005 for the 6 simulations that best agree with observations (lowest error score).

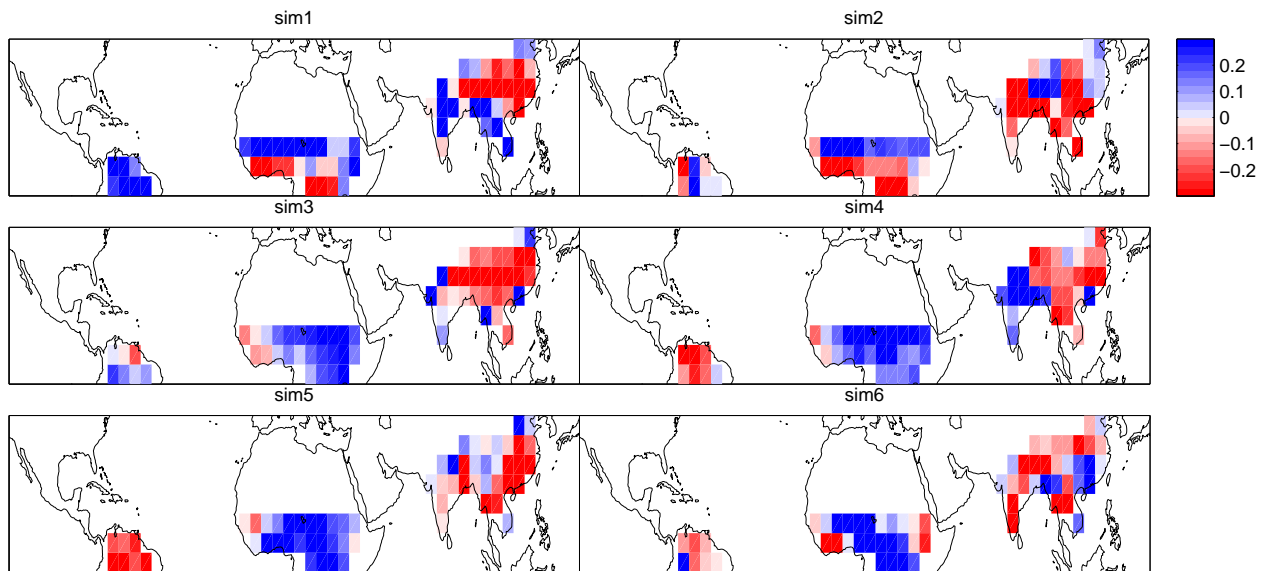


FIG. S10. Linear trends for simulations with least agreement with observations. ALL forced simulation MJJAS precipitation linear trends (mm/day/year) for 1951-2005 for 6 simulations with least agreement with observations (highest error score).

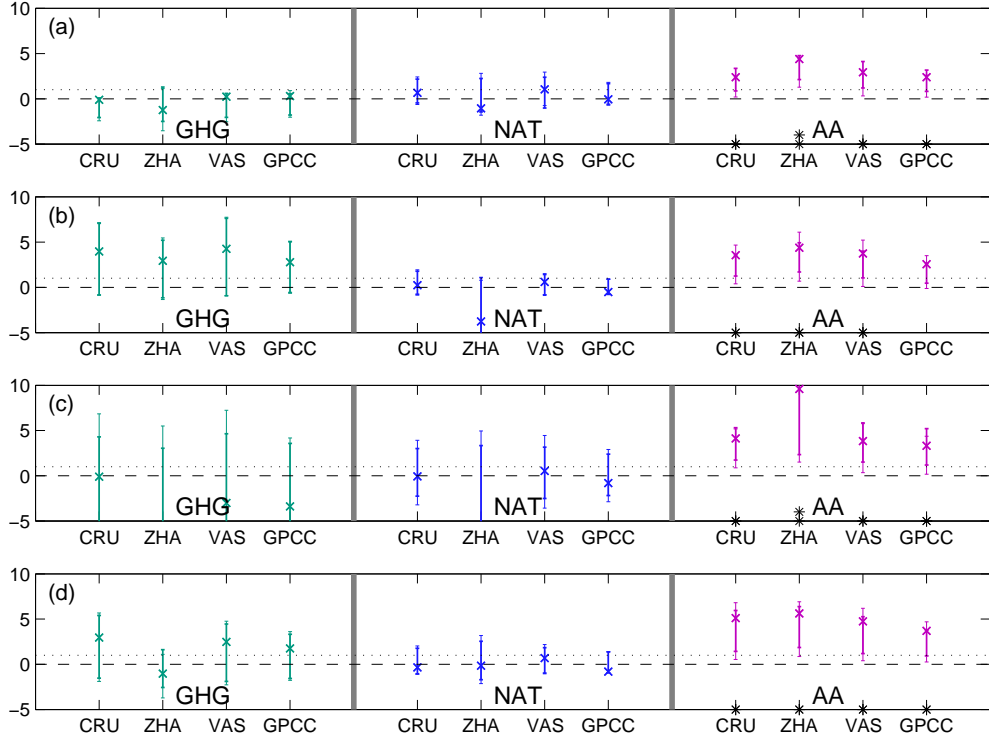


FIG. S11. Detection and attribution results for observed changes in NHSM precipitation testing for overweighting of individual regions. Shown are the 3-signal analysis results for greenhouse gas (GHG), natural (NAT) and anthropogenic aerosol (AA) forcing for the NHSM region (a)-(c), excluding South American, African and Asian monsoon regions and (d), including the mid-latitude regions. Results are shown for four observational datasets, CRU (CRU), Zhang (ZHA), VasClimO (VAS) and GPCP (GPCC). Crosses show the best-guess scaling factor for the multi-model mean, thick lines are the 90% confidence interval based on the raw variance and thin lines are the 90% confidence intervals when model variance has been doubled. The residual consistency test is passed for all cases. Stars (*) show where forcing is detected and two stars show where forcing is detected but inconsistent with a scaling factor of 1.

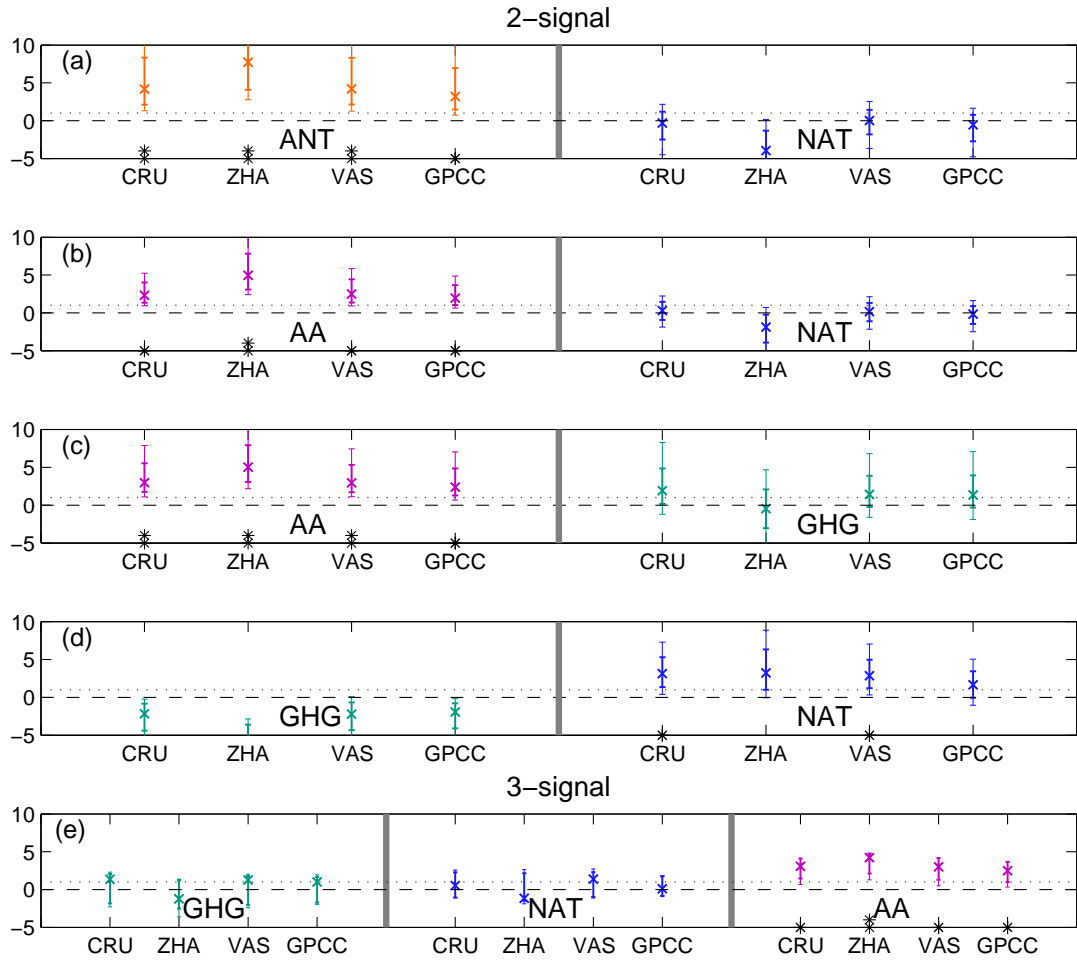


FIG. S12. Detection and attribution results for observed changes in NHSM precipitation where the same models are used to produce the fingerprint for each combination of forcings. (a)-(d), 2-signal and (e), 3-signal detection and attribution analysis. (a), anthropogenic (ANT) and natural (NAT) forcing, (b), anthropogenic aerosol (AA) and natural (NAT) forcing, (c), anthropogenic aerosol (AA) and greenhouse gas (GHG) forcing, (d), greenhouse gas (GHG) and natural (NAT) forcing and (e), greenhouse gas (GHG), natural (NAT) and anthropogenic aerosol (AA) forcing. Results are shown for four observational datasets, CRU (CRU), Zhang (ZHA), VasClimO (VAS) and GPCP (GPCC). Crosses show the best-guess scaling factor for the multi-model mean, thick lines are the 90% confidence interval based on the raw variance and thin lines are the 90% confidence intervals when model variance has been doubled. The residual consistency test is passed for all cases. Stars (*) show where forcing is detected and two stars show where forcing is detected but inconsistent with a scaling factor of 1.

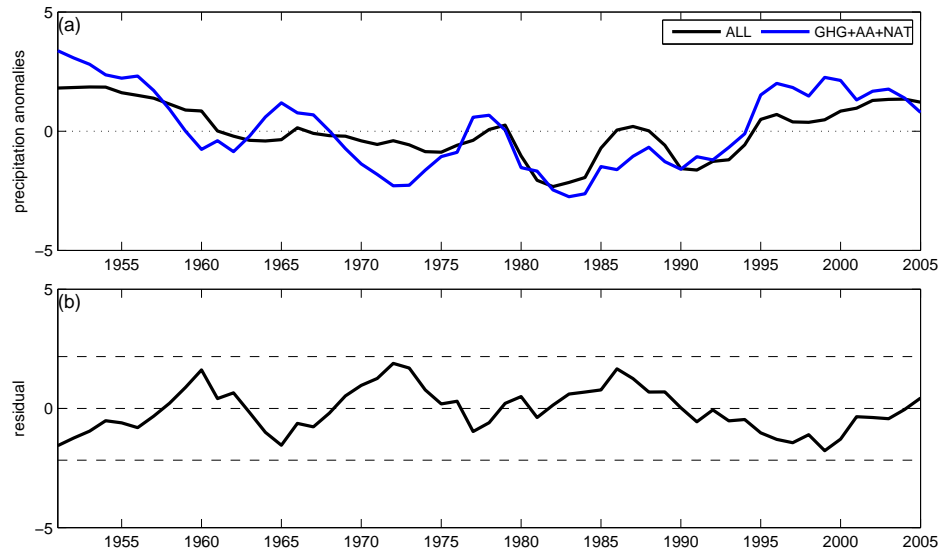


FIG. S13. Test of linearity assumption (a), The ALL multi-model mean and the sum of GHG+NAT+AA multi-model means for the NHSM region. (b), Residual (ALL multi-model mean minus the summed GHG+NAT+AA multi-model means). Dashed lines show 2 standard deviations of the internal variability from noise sample ensemble derived from the ALL forcing ensemble.

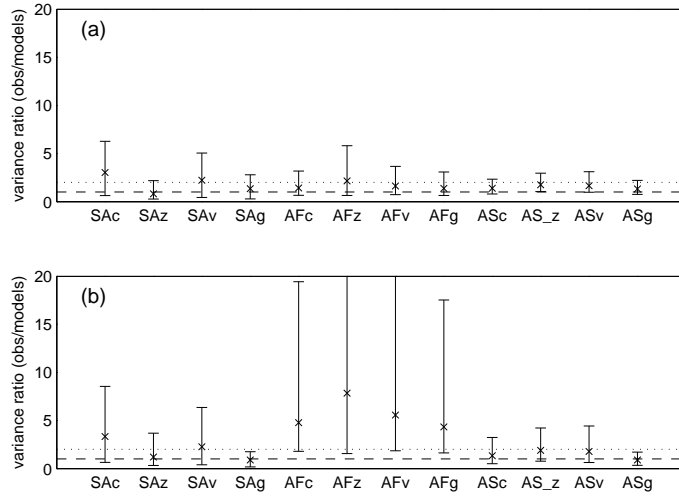


FIG. S14. Comparison of observed and modelled variance. Ratio of observed and ALL forced model simulations mean MJJAS precipitation variance for each region, SA is South America, AF is Africa and AS is Asia) and each observational datasets (c is CRU, z is Zhang v is VasClimO and g is GPCC). (a) unsmoothed, (b) 9-year running mean. The crosses show the median value and the bars are the 90% confidence interval. Dashed lines shows ratio of 1 and dotted line shows ratio of 2.